Optical creation and annihilation of skyrmion patches in a chiral magnet

J. Kalin,* S. Sievers, H.W. Schumacher, R. Abram, H. Füser, and M. Bieler
Physikalisch-Technische Bundesanstalt, Braunschweig 38116, Germany

D. Kalin
ESE Engineering und Software-Entwicklung GmbH, Braunschweig 38122, Germany

A. Bauer
Physik-Department, Technische Universität München, Garching 85748, Germany
and Zentrum für QuantumEngineering (ZQE),
Technische Universität München, Garching 85748, Germany

C. Pfleiderer
Physik-Department, Technische Universität München, Garching 85748, Germany
Zentrum für QuantumEngineering (ZQE),
Technische Universität München, Garching 85748, Germany
and Munich Center for Quantum Science and Technology (MCQST),
Technische Universität München, Garching 85748, Germany

(Received 3 June 2023; revised 14 January 2024; accepted 27 February 2024; published 29 March 2024)

A key challenge for the realization of future skyrmion devices comprises the controlled creation, annihilation, and detection of these topologically nontrivial magnetic textures. In this study, we report an all-optical approach for writing, deleting, and reading skyrmions in the chiral magnet $Fe_{0.75}Co_{0.25}Si$ based on thermal quenching. Using focused femtosecond laser pulses, patches of a thermally metastable skyrmion lattice state are created and annihilated locally, demonstrating unprecedented control of skyrmions in chiral magnets. The skyrmion state is read out by analyzing the microwave spin excitations in time-resolved magneto-optical Kerr effect measurements. Extracting the magnetic field and laser-fluence dependence, we find well-separated magnetic field regimes and different laser-fluence thresholds for the laser-induced creation and annihilation of skyrmions. The all-optical skyrmion control, as established in this study for a model system, represents a promising and energy-efficient approach for the realization of skyrmions as magnetic bits in future storage devices, reminiscent of magneto-optical storage devices in the past.

DOI: 10.1103/PhysRevApplied.21.034065

The formation of skyrmions, i.e., nanometer-sized magnetic whirls, from a topologically trivial magnetic state requires topological winding to build up the skyrmion's inherent structure. Consequently, once formed, skyrmions tend to be remarkably robust, as characterized by long characteristic time scales for skyrmion unwinding [1]. In chiral magnets, skyrmions are typically observed as an equilibrium state within a narrow parameter range of the magnetic phase diagram at temperatures just below the onset of long-ranged magnetic order [2], where they align in a hexagonal lattice [3]. However, the large characteristic time scales for skyrmion unwinding allow creation of a metastable skyrmion lattice state (MSkL) across larger parts of the phase diagram by thermal quenching [4–13]. Most notably, recent studies on thin lamellas of chiral magnets demonstrated the creation and even the annihilation of MSkL through the uniform irradiation with femtosecond (fs) laser pulses [14,15], using a laser-beam diameter significantly larger than the sample size. The MSkL forms predominately at defects and the sample edges [14], resulting in either the coexistence of MSkL with the equilibrium state [14] or the formation of a uniform MSkL [15], both extending over the entire lamella. The laser-induced creation [16–21] and annihilation [17] of skyrmions has been accomplished also in ferromagnetic multilayer systems, in which single skyrmions or multiple unordered skyrmions are formed. These observations establish that laser light can trigger topological winding or unwinding processes and, thus, topological phase transitions, promising for fast and energy-efficient [22] all-optical skyrmion devices featuring optical writing, deleting, and reading operations. So far, however, the laser-induced creation and annihilation of skyrmions has not been combined with optical readout techniques.

*jantje.kalin@ptb.de

In this paper, we demonstrate the all-optical manipulation of a spatially confined MSkL in the chiral magnet $Fe_{0.75}Co_{0.25}Si$. By local irradiation of the sample with fs laser pulses, employing a laser-beam diameter much smaller than the sample size, the magnetic state of the chiral magnet is controlled locally, most notably, a patch of MSkL embedded in the equilibrium conical phase is created or annihilated. We systematically track the MSkL patch in time-resolved magneto-optical Kerr effect (TR-MOKE) measurements, establishing an optical readout technique. We find laser-induced MSkL creation and annihilation in distinct and well-separated magnetic field regimes for different laser-fluence thresholds, reflecting the temperature regimes for the stabilization and destabilization of the MSkL. Overall, this study demonstrates the feasibility of all-optical skyrmion read-write-delete operations within a single experimental framework, promising potential for applications in fields such as data storage [23–25], microwave [26,27], or neuromorphic computing [28–31].

We accomplish laser-induced creation and annihilation of a MSkL patch on a bulk sample of the chiral magnet $Fe_{0.75}Co_{0.25}Si$. This material exhibits the generic magnetic phase diagram of cubic chiral magnets [5], displayed in Fig. 1(a). While being a paramagnet (PM) for temperatures above the ordering temperature $T_c = 39$ K, magnetic order sets in for $T < T_c$ comprising long-range helimagnetism (H), conical order, and a field-aligned (FA) state under increasing magnetic field [32]. Note, that in the doped semiconductor $Fe_{1-x}Co_xSi$ the helical phase is only stabilized, when the phase regime of the conical phase is not crossed during cooldown [32]. This condition is satisfied during zero-field cooling (cooldown at $\mu_0 H = 0$ T). Otherwise, the conical phase persists down to zero magnetic fields. Of note, in a limited temperature and magnetic field range just below T_c, a hexagonal lattice of skyrmions (SkL) [3] is observed. Previous studies [4–12] established that thermal quenching under magnetic fields crossing the SkL may avoid the equilibrium phase transition between the skyrmion lattice and conical phase kinetically, resulting in a MSkL extending over large parts of the magnetic phase diagram, see Fig. 1(b). The characteristic time scale for MSkL unwinding exponentially increases with decreasing temperature and also depends on the applied magnetic field [1]. When the magnetic field is outside the SkL range, an increase in temperature gradually induces the decay of the MSkL through skyrmion unwinding on experimentally relevant time scales. This thermal destabilization of the MSkL results in the full transition to the conical phase at $T_{\rm con}$, see Fig. 1(b). So far, for bulk chiral magnets a MSkL was realized by uniform thermal quenching of the whole sample [5,7,8,10,11], leading to a MSkL that spans the entire crystal. This was achieved through techniques such as rapid field cooling [5,8,10,11], where the sample is cooled at high cooling rates from temperatures above

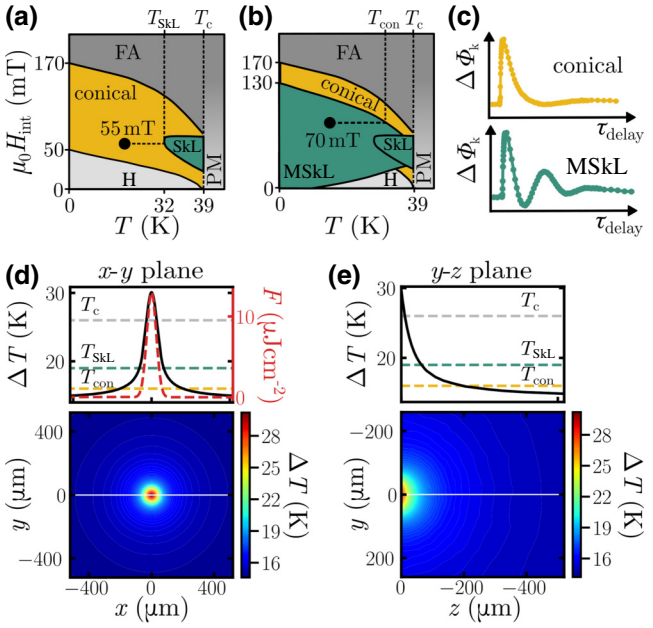

FIG. 1. Schematic magnetic phase diagram of $Fe_{0.75}Co_{0.25}Si$ (a) in thermal equilibrium and (b) following thermal quenching through the SkL. (c) Characteristic out-of-plane magnetization dynamics of $Fe_{0.75}Co_{0.25}Si$ in the equilibrium conical phase (top panel) and the MSkL (bottom panel) measured in TR-MOKE experiments as Kerr angle change ($\Delta\phi_k$) as a function of the time delay $\tau_{\rm delay}$ between pump and probe beam at 13 K and 55 mT. (d),(e) Simulated temperature distribution in steady state after laser heating with $F = 13$ μJ cm^{-2} at $T = 13$ K in the x-y plane being equal to the sample surface and in the y-z plane. The upper graphs in (d),(e) show the temperature distributions along the white lines indicated in the lower graphs and compare them to characteristic temperature values [T_c, $T_{\rm SkL}$(55 mT), $T_{\rm con}$(70 mT)]. In (d) the fluence profile of the Gaussian laser beam (red dashed line) is depicted for estimating effects of thermal diffusion. Further information on the thermal simulations can be found in Ref. [37].

T_c to lower temperatures using cryogenic temperature control.

In a recent study [11], it was established that TR-MOKE measurements provide a sensitive probe for MSkL detection, accomplished by comparing the out-of-plane magnetization dynamics of the equilibrium conical phase with that of the MSkL, as stabilized through rapid field cooling. In the equilibrium conical phase, shown in the upper panel of Fig. 1(c) for our sample, a nonoscillatory de- and remagnetization characteristic is observed. In contrast, in the MSkL, at the same magnetic field and temperature, the skyrmion breathing mode [33–35] is detected as a precessional signal, as seen in the lower panel of Fig. 1(c).

In this work, we adopt this approach to probe the laser-induced creation and annihilation of MSkL by performing TR-MOKE measurements in a pump-probe

experiment. We apply laser pulses of about $\tau_{\text{pulse}} = 150$ fs duration with a center wavelength of $\lambda = 800$ nm and a repetition rate of $G = 76$ MHz to the single-crystal $Fe_{0.75}Co_{0.25}Si$ with size of $(2 \times 2 \times 2)$ mm^3. The concentrical pump pulses with focal $1/e^2$ radius of 60 μm and probe pulses with focal $1/e^2$ radius of $w_L = 30$ μm are focused under near-normal incidence onto the surface of the sample. The sample is located in an optical cryostat with the magnetic field pointing out of the sample plane parallel to the ⟨100⟩ crystallographic direction. The linearly polarized pump beam thermally triggers the magnetization dynamics of the sample. The dynamics is detected via the polarization change of the reflected probe beam as induced by the MOKE, i.e., by measuring the Kerr rotation $\Delta\phi_k$ in a stroboscopic manner as a function of the time delay τ_{delay} between probe and pump beam. As the laser light penetrates approx. 30 nm [36] into the $Fe_{0.75}Co_{0.25}Si$ sample, TR-MOKE is sensitive to the magnetization dynamics in the sample surface only. The measurement technique is discussed in more detail in Ref. [11]. For a noninvasive detection of the magnetic states we choose the lowest possible pump laser fluence for the TR-MOKE measurements $F = 2.2$ μJ cm^{-2} to limit the temperature increase by steady-state heating to about 5 K.

Complementing the observation of a MSkL in chiral magnets after uniform thermal quenching in previous studies [4–12], in this work, a local heating and cooling process was implemented in terms of a series of high-fluence fs laser pulses. Experimentally, this is realized by temporarily increasing the laser fluence of the TR-MOKE pump beam (irradiation of the sample with approximately equal to 2×10^6 laser pulses), while keeping all other laser parameters unchanged. The cumulative heat load of the high-fluence laser pulses leads to a local increase of the sample temperature in a spatially confined volume in the vicinity of the laser focal spot, as shown by thermal simulations in Figs. 1(d) and 1(e). This volume has a micrometer-sized extension along the surface as well as perpendicular to it and thus is significantly smaller than the sample. After reducing the laser fluence again, the local temperature rise is rapidly compensated by the thermal reservoir provided by the cryostat resulting in a fast and nonuniform sample cooling.

As a first implementation of this local heating and cooling process, we start in the conical phase at 13 K and 55 mT, see circle in Fig. 1(a), and apply high-fluence laser pulses of $F = 13$ μJ cm^{-2} to the sample. The magnetic state is probed spatially resolved in TR-MOKE experiments before and after the irradiation with the high-fluence laser pulses. Figure 2(a) exemplarily shows the magnetization dynamics at four sample positions with different distances d to the center of the laser irradiation spot. Prior to exposing the sample to high-fluence laser pulses, we measure at all positions the dynamics of the conical phase, as indicated by the gray symbols in Fig. 2(a). In proximity to the irradiation spot, i.e., for $d <$ 140 μm, the magnetization dynamics undergo a change upon exposure to high-fluence laser pulses, displaying precessional dynamics with distance-dependent amplitude. Such dynamics is characteristic for the skyrmion breathing mode of the MSkL, as confirmed through a comparison to the dynamics in Fig. 1(c) and by analyzing its dispersion [37]. We attribute the distance-dependent amplitude of the precessional signal to a mixed state of MSkL and conical phase formed in the laser-heated area, as addressed later in the text. For $d \geqslant 140$ μm the initial conical phase persists after the irradiation with the high-fluence laser pulses. Therefore, the presented data establish that local laser irradiation of a chiral magnet can drive a conical-to-MSkL transition selectively in a confined area of the sample. Unlike earlier investigations on thin lamellas of chiral magnets [14,15], we demonstrate the laser-induced creation of a MSkL patch, while the majority of the sample retains its equilibrium conical phase. The laser-written MSkL patch persists over long time scales (>12 h, not shown) and has a comparable magnetic field and temperature stability as the uniform MSkL created by rapid field cooling [37]. This demonstrates that the interfaces between the equilibrium conical phase and MSkL patch are stable on experimentally relevant time scales. Accordingly, the conical background does not act as nucleus for triggering skyrmion unwinding [1]. We observe laser-induced MSkL creation selectively for magnetic fields in the regime of the SkL [37]. Therefore, we ascribe the formation of the laser-written MSkL patch in $Fe_{0.75}Co_{0.25}Si$ to local thermal quenching of the equilibrium SkL by laser heating.

In Fig. 2(b) we show that by local laser irradiation of $Fe_{0.75}Co_{0.25}Si$ laser-induced MSkL annihilation can be implemented as well. Following the formation of a MSkL by means of rapid field cooling to 13 K, the magnetization dynamics are studied before and after irradiation with high-fluence laser pulses with $F = 13$ μJ cm^{-2} at 70 mT, i.e., at a magnetic field above the SkL pocket, see circle in Fig. 1(b). Prior to the irradiation, the characteristic dynamics of the MSkL are observable across the entire sample, as indicated by the plots with gray circles in Fig. 2(b), demonstrating that rapid field cooling leads to a MSkL state that spans the whole sample. In a situation reverse to laser-induced MSkL creation, we observe a local formation of the conical phase in proximity to the irradiation spot after high-fluence laser exposure at 70 mT, as shown in Fig. 2(b). Again, the observed dynamics suggest the formation of a mixed state of the conical phase and MSkL in the laser-heated area, as evident by small precessional signals in the TR-MOKE measurements for short distances d. For $d > 200$ μm, magnetization dynamics of the initial MSkL is detected. Consequently, laser-induced MSkL annihilation is achieved after local irradiation of the $Fe_{0.75}Co_{0.25}Si$ sample, forming a conical patch in a MSkL

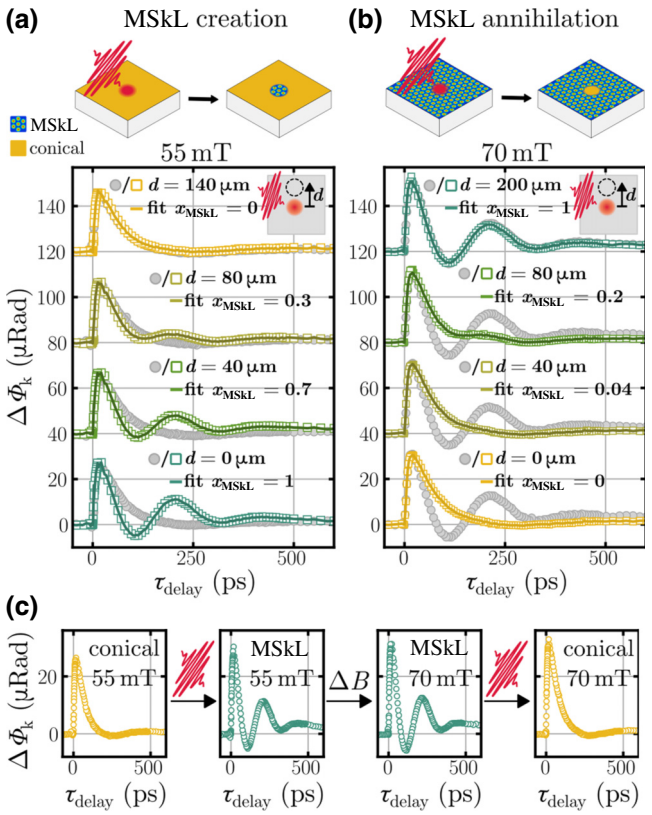

FIG. 2. Magnetization dynamics of $Fe_{0.75}Co_{0.25}Si$ measured at different distances d from the irradiation spot before (gray circles) and after (colored squares) high-fluence laser irradiation with $F = 13\ \mu J\ cm^{-2}$ at 13 K: (a) starting in the conical phase at 55 mT, and (b) in the MSkL, formed through rapid field cooling, at 70 mT. The solid lines represent fits to the experimental data using Eq. (1). High-fluence laser pulses are applied at the same sample position in (a),(b). Data for $d > 0$ µm have been offset by multiples of 40 µRad for clarity. (c) Sequence for all-optical MSkL control in $Fe_{0.75}Co_{0.25}Si$: a laser-written MSkL state, formed through high-fluence irradiation of the conical phase at 55 mT, is laser annihilated at 70 mT.

background. A switching from MSkL to the conical phase after laser irradiation occurs exclusively for magnetic field values outside the equilibrium SkL [37]. Thus, we attribute the laser-induced annihilation of the MSkL to its thermal destabilization by laser heating.

These findings show that laser-induced MSkL creation and annihilation in $Fe_{0.75}Co_{0.25}Si$ takes place in well-defined and separated magnetic field regimes. As illustrated in Fig. 2(c), this allows us to realize all-optical MSkL creation and annihilation sequences with readout operation controlled by the applied magnetic field. A laser-written MSkL patch generated through high-fluence laser exposure within the field regime of the SkL, can be annihilated again by subjecting it to high-fluence laser pulses at magnetic fields outside the field regime of the SkL, promising from an application point of view.

The results presented so far indicate that laser-induced MSkL creation and annihilation leads to the formation of mixed states of MSkL and the conical phase in the laser-heated area and thus to a gradual magnetic phase transition in this region. To study this aspect further, the spatially resolved measurements in Figs. 2(a) and 2(b) are modeled by a linear superposition of the conical, $\Delta\phi_{k,\mathrm{conical}}$, and MSkL, $\Delta\phi_{k,\mathrm{MSkL}}$, contributions to the measured signal

$$\Delta\phi_k(\tau_{\mathrm{delay}}) = x_{\mathrm{MSkL}} \cdot \Delta\phi_{k,\mathrm{MSkL}}(\tau_{\mathrm{delay}}) + (1 - x_{\mathrm{MSkL}}) \cdot \Delta\phi_{k,\mathrm{conical}}(\tau_{\mathrm{delay}}). \quad (1)$$

As the TR-MOKE technique averages over magnetization dynamics in the probed area and is only sensitive to the sample surface, the MSkL ratio x_{MSkL} describes the areal percentage of MSkL in the probed region. The line plots in Figs. 2(a) and 2(b) are fits to the experimental data using Eq. (1) with x_{MSkL} as the fitting parameter, showing excellent agreement with the data. By plotting x_{MSkL} as a function of distance d from the laser irradiation spot center, as shown in Figs. 3(a) and 3(b) after laser irradiation with different fluences F, the spatial dimensions of the patches of laser-induced MSkL creation and annihilation can be determined quantitatively.

Extracting the spatial MSkL distribution $\rho_{\mathrm{MSkL}}(r)$ requires $x_{\mathrm{MSkL}}(d)$ to be deconvolved with the intensity profile of the probe beam $I(r+d)/I_0$ [37] to take into account the spatial averaging of TR-MOKE. The spatial MSkL distribution after laser-induced MSkL creation is best described by a higher-order Gaussian function given

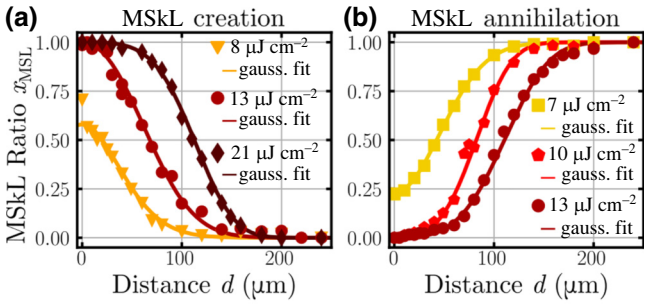

(c)

F (µJ cm^{-2})	8	13	21
ρ_0	0.58	1	1
w_{MSkL} (µm)	75	105	142
n	1.7	2.3	4.6

(d)

F (µJ cm^{-2})	7	10	13
ρ_0	0.23	1	1
w_{MSkL} (µm)	86	108	145
n	2	3.8	3.9

FIG. 3. MSkL ratio x_{MSkL} in the probed area as a function of the distance to the irradiation spot for (a) laser-induced MSkL creation and (b) annihilation after high-fluence irradiation with different laser fluences. The solid lines represent fits to the experimental data using the model introduced in the main text. (c),(d) Fit parameters leading to the best agreement between model and data for MSkL creation and annihilation, respectively.

by

$$\rho_{\mathrm{MSkL}}(r) = \rho_0 \times \exp\left(\frac{-2|r|^n}{|w_{\mathrm{MSkL}}|^n}\right), \qquad (2)$$

with radius w_{MSkL}, corresponding to the distance r from the center of the laser irradiation spot where ρ_{MSkL} drops to $1/e^2$. Here, ρ_0 describes the MSkL density in the center of the laser irradiation spot at $r = 0$. For laser-induced MSkL annihilation, the MSkL distribution is given by $1 - \rho_{\mathrm{MSkL}}(r)$. The line plots in Figs. 3(a) and 3(b) show that the experimental data can be well approximated with the chosen model using w_{MSkL}, n, and ρ_0 as fit parameters.

In Figs. 3(c) and 3(d) we summarize the fit parameters leading to the best agreement between the model and data. The radius w_{MSkL} increases with the laser fluence and gets larger than the laser focal width for high fluences, consistent with sizable thermal diffusion, see Fig. 1(d). Moreover, the shape of the MSkL distribution changes with laser fluence. Irradiation with smaller laser fluence results in the formation of a Gaussian MSkL distribution ($n \leq 2$), shown for 8 and 7 μJ cm^{-2} for laser-induced MSkL creation and annihilation in Figs. 3(a) and 3(b), respectively. For higher laser fluence, the MSkL distribution forms a flat top ($n > 2$) that broadens under further increasing laser fluences. The spatial MSkL distribution ρ_{MSkL} differs for laser-induced creation and annihilation as reflected by different w_{MSkL} and n. Most notably, for the same irradiation fluence of 13 μJ cm^{-2}, the MSkL is annihilated in a larger region than it is created, leading to different patch sizes of laser-induced MSkL creation ($w_{\mathrm{MSkL}} = 105$ μm) and annihilation ($w_{\mathrm{MSkL}} = 145$ μm).

This finding implies the need to investigate the fluence dependence of these processes, which we accomplish by analyzing the magnetization dynamics after irradiation with laser pulses of different fluences at $d = 0$ μm. Figures 4(a) and 4(b) show TR-MOKE measurements after laser irradiation with four different laser fluences starting in the equilibrium conical phase (55 mT, 13 K) and the laser-written MSkL (70 mT, 13 K), respectively. With increasing fluence, the magnetization dynamics gradually evolves from the characteristic behavior of the conical phase to that of the MSkL and vice versa. Again, the measurements are described well by Eq. (1), as shown by the good agreement of the fits and the data in Figs. 4(a) and 4(b).

The resulting MSkL ratio x_{MSkL} as a function of the irradiation fluence is shown in Figs. 4(c) and 4(d) for MSkL creation and annihilation, respectively, and two different temperatures. We observe a double-threshold behavior for laser-induced MSkL creation (F_{t1}, F_{t2}) and annihilation ($F_{\mathrm{t1}}^{\dagger}$, $F_{\mathrm{t2}}^{\dagger}$). The laser-induced magnetic phase transition sets in for fluences larger than a lower threshold $F_{\mathrm{t1}}^{(\dagger)}$ and completes above an upper fluence threshold $F_{\mathrm{t2}}^{(\dagger)}$. In the fluence regime between $F_{\mathrm{t1}}^{(\dagger)}$ and $F_{\mathrm{t2}}^{(\dagger)}$ the MSkL

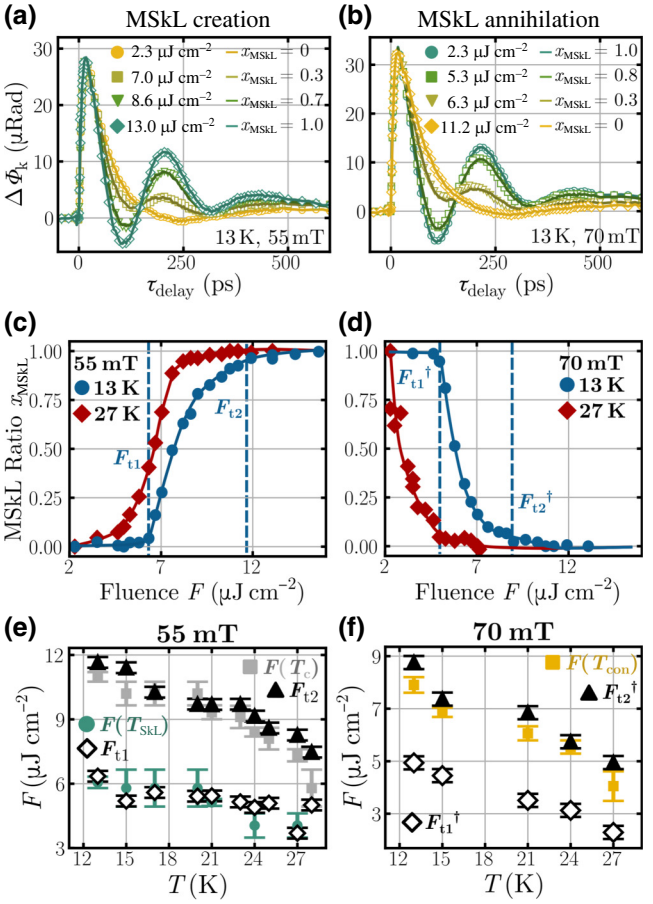

FIG. 4. Magnetization dynamics of $Fe_{0.75}Co_{0.25}Si$ after irradiation with laser pulses of different fluences starting in (a) the equilibrium conical phase, and (b) the MSkL at $d = 0$ μm. The solid lines in (a),(b) represent fits to the experimental data using Eq. (1). MSkL ratio x_{MSkL} as a function of irradiation fluence for (c) laser-induced MSkL creation and (d) annihilation at 13 and 27 K. The dashed blue lines show the 5% and 95% fluence thresholds at 13 K. (e),(f) Comparison of the laser fluence F, required to raise the sample temperature to T_c (gray squares), T_{SkL} (turquoise circles), and T_{con} (yellow squares), with the fluence thresholds of (e) laser-induced MSkL creation (open diamonds for F_{t1}, black triangles F_{t2}) at 55 mT, and (f) annihilation (open diamonds for $F_{\mathrm{t1}}^{\dagger}$, black triangles for $F_{\mathrm{t2}}^{\dagger}$) at 70 mT for various start temperatures.

ratio x_{MSkL} increases with the irradiation fluence. Thus, for fluences smaller than $F_{\mathrm{t2}}^{(\dagger)}$, the laser irradiation leads to only a partial switching between MSkL and equilibrium conical phase and to a coexistence of both states with a fluence-dependent MSkL ratio. This finding agrees well with previous studies on laser-induced creation of skyrmions [14,15,17], which also showed a coexistence of metastable skyrmions and the equilibrium state after laser irradiation.

In Figs. 4(c) and 4(d) the fluence thresholds $F_{\mathrm{t1}}^{(\dagger)}$ and $F_{\mathrm{t2}}^{(\dagger)}$, defined as 5% and 95% switching ratios toward

the final state, are shown for 13 K as dashed vertical lines. The fluence thresholds for laser-induced MSkL creation at this temperature are $F_{t1} = 6.4\ \mu J\ cm^{-2}$ and $F_{t2} = 11.7\ \mu J\ cm^{-2}$, while for MSkL annihilation, they are $F_{t1}^{\dagger} = 4.9\ \mu J\ cm^{-2}$ and $F_{t2}^{\dagger} = 8.8\ \mu J\ cm^{-2}$. Thus, the annihilation of the MSkL sets in and completes at lower fluences than the creation process at the same temperature. With that, the different patch sizes of laser-induced MSkL creation and annihilation can be traced back to the different fluence dependencies. Namely, by irradiation with the same laser fluence the lower threshold for MSkL annihilation is exceeded in a larger area than the higher threshold for MSkL creation, due to the spatial Gaussian fluence profile of the laser beam. Similarly, the transition from a Gaussian to a flat-top spatial MSkL distribution, characterized by an increase of n in Eq. (2) relates to the saturation of the final state at $d = 0\ \mu m$ when locally reaching the threshold $F_{t2}^{(\dagger)}$, as shown in Figs. 4(c) and 4(d).

Moreover, Figs. 4(c) and 4(d) demonstrate that the fluence thresholds of laser-induced MSkL creation and annihilation decreases at higher temperatures, as evidenced by the comparison of $x_{MSkL}(F)$ at 13 and 27 K. This is consistent with the laser-induced temperature rise in the material being key for MSkL creation and annihilation. To quantitatively assess the relationship between this temperature rise and the fluence thresholds, we estimate the local temperature increase caused by laser heating by comparing fluence and temperature-dependent TR-MOKE measurements [37]. In Fig. 4(e), the laser fluences $F(T_{SkL})$ and $F(T_c)$ leading to a local increase of the sample temperature to T_{SkL} and T_c, respectively, are compared to the lower F_{t1} (white diamonds) and upper F_{t2} (black triangle) fluence threshold of laser-induced MSkL creation. Here, T_{SkL} represents the lowest temperature within the SkL regime for a given magnetic field, as illustrated in Fig. 1(a). The comparison reveals that F_{t1} and F_{t2} correspond to a local temperature increase to T_{SkL} and T_c, respectively, which aligns well with laser-induced MSkL creation due to local thermal quenching of the equilibrium SkL. The increase of the MSkL ratio in the fluence regime from F_{t1} to F_{t2}, i.e., for higher temperature rises in the SkL, might be attributed to the proliferation of the topological winding process for temperatures approaching T_c. This influences the probability of SkL stabilization and consequently affects the number of skyrmions preserved following laser heating.

In Fig. 4(f), the laser fluence $F(T_{con})$ leading to a local increase of the sample temperature to T_{con} and the fluence thresholds of laser-induced annihilation are plotted as a function of temperature. In agreement with the phase diagram shown the Fig. 1(b), the upper threshold of MSkL annihilation $F_{t2}^{\dagger}$ corresponds to a local temperature increases to T_{con}. This behavior is consistent with laser-induced MSkL annihilation due to local transient laser heating of the sample to temperatures that destabilize the MSkL and lead to the formation of the conical phase. Additionally, the data in Fig. 4(f) demonstrate that even temperature rises much smaller than T_{con} are sufficient to partially switch from MSkL to the conical phase, as $F_{t1}^{\dagger}$ is much smaller than $F(T_{con})$. This is attributed to the temperature-dependent lifetime of the MSkL [1]. As temperature increases the MSkL lifetime decreases, resulting in an increased transition probability between the MSkL and conical phase during high-fluence laser irradiation.

Our laser heating simulations in Fig. 1(e) indicate substantial heat penetration perpendicular to the sample surface, leading to a rise of the sample temperature to T_c, T_{SkL}, and T_{con} at micrometer distances to the sample surface. Following the analysis above, such a temperature distribution suggests that laser-induced MSkL creation and annihilation are not confined to the sample surface, but may extend to a micrometer-sized volume in the sample. Thus, also the chiral ordering of the skyrmions in the laser-written MSkL may continue into the bulk material on a finite micrometer scale, a detail not captured by our surface-sensitive measurement technique. In future studies, TR-MOKE measurements could investigate this aspect by simultaneously probing the front and back of a micrometer-scale sample.

In summary, our study explored the all-optical manipulation of a MSkL patch in the chiral magnet $Fe_{0.75}Co_{0.25}Si$. By probing the magnetization dynamics in TR-MOKE experiments, we demonstrate laser-induced MSkL creation and annihilation in spatially-confined areas for well-defined magnetic field regimes. Spatially-resolved and fluence-dependent measurements indicate that creation and annihilation in $Fe_{0.75}Co_{0.25}Si$ are linked to distinct temperature regimes for the stabilization and destabilization of the MSkL. These results provide promising steps towards the all-optical local control of skyrmions for a fast and energy efficient manipulation in future storage, microwave, or neuromorphic computing devices, as well as insights into optically induced local topological phase transitions in terms of thermal quenching.

All data needed to evaluate the conclusions of the paper are present in the paper and in the Supplemental Material.

ACKNOWLEDGMENTS

This work was supported by the European Metrology Research Programme (EMRP) and EMRP participating countries under the European Metrology Programme for Innovation and Research (EMPIR) Project No. 17FUN08-TOPS Metrology for topological spin structures. In part, this study has been funded by the Deutsche Forschungsgemeinschaft (DFG, German ResearchFoundation) under TRR80 (From Electronic Correlations to Functionality,

Project No. 107745057, Project E1), SPP2137 (Skyrmionics, Project No. 403191981, Grant No. PF393/19 and Grant No. SCHU 2250/8-1), the excellence cluster MCQST under Germany's Excellence Strategy EXC-2111 (Project No. 390814868) and EXC-2123 QuantumFrontiers (Project No. 390837967). Financial support by the European Research Council (ERC) through Advanced Grants No. 291079 (TOPFIT) and No. 788031 (ExQuiSid) is gratefully acknowledged.

J.K. initiated the study. A.B. and C.P. grew the crystal. J.K. performed the TR-MOKE study under the supervision of M.B. and H.F. The data analysis was carried out by J.K. D.K. and R.A. supported the study with simulations. All authors discussed the results. J.K. wrote the paper with comments of all authors.

The authors declare that they have no competing interests.

[1] J. Wild, T. N. G. Meier, S. Pöllath, M. Kronseder, A. Bauer, A. Chacon, M. Halder, M. Schowalter, A. Rosenauer, J. Zweck *et al.*, Entropy-limited topological protection of skyrmions, Sci. Adv. **3**, e1701704 (2017).

[2] S. Mühlbauer, B. Binz, F. Jonietz, C. Pfleiderer, A. Rosch, A. Neubauer, R. Georgii, and P. Böni, Skyrmion lattice in a chiral magnet, Science **323**, 915 (2009).

[3] X. Z. Yu, Y. Onose, N. Kanazawa, J. H. Park, J. H. Han, Y. Matsui, N. Nagaosa, and Y. Tokura, Real-space observation of a two-dimensional skyrmion crystal, Nature **465**, 901 (2010).

[4] Y. Okamura, F. Kagawa, S. Seki, and Y. Tokura, Transition to and from the skyrmion lattice phase by electric fields in a magnetoelectric compound, Nat. Commun. **7**, 1 (2016).

[5] W. Münzer, A. Neubauer, T. Adams, S. Mühlbauer, C. Franz, F. Jonietz, R. Georgii, P. Böni, B. Pedersen, M. Schmidt *et al.*, Skyrmion lattice in the doped semiconductor $Fe_{1-x}Co_xSi$, Phys. Rev. B **81**, 041203(R) (2010).

[6] A. Bauer, A. Chacon, M. Halder, and C. Pfleiderer, in *Topology in Magnetism* (Springer, 2018), p. 151.

[7] H. Oike, A. Kikkawa, N. Kanazawa, Y. Taguchi, M. Kawasaki, Y. Tokura, and F. Kagawa, Interplay between topological and thermodynamic stability in a metastable magnetic skyrmion lattice, Nat. Phys. **12**, 62 (2016).

[8] L. J. Bannenberg, K. Kakurai, F. Qian, E. Lelièvre-Berna, C. D. Dewhurst, Y. Onose, Y. Endoh, Y. Tokura, and C. Pappas, Extended skyrmion lattice scattering and long-time memory in the chiral magnet $Fe_{1-x}Co_xSi$, Phys. Rev. B **94**, 104406 (2016).

[9] R. Takagi, M. Garst, J. Sahliger, C. H. Back, Y. Tokura, and S. Seki, Hybridized magnon modes in the quenched skyrmion crystal, Phys. Rev. B **104**, 144410 (2021).

[10] S. Seki, M. Garst, J. Waizner, R. Takagi, N. D. Khanh, Y. Okamura, K. Kondou, F. Kagawa, Y. Otani, and Y. Tokura, Propagation dynamics of spin excitations along skyrmion strings, Nat. Commun. **11**, 1 (2020).

[11] J. Kalin, S. Sievers, H. Füser, H. W. Schumacher, M. Bieler, F. García-Sánchez, A. Bauer, and C. Pfleiderer, Optically excited spin dynamics of thermally metastable skyrmions in $Fe_{0.75}Co_{0.25}Si$, Phys. Rev. B **106**, 054430 (2022).

[12] P. Milde, D. Köhler, J. Seidel, L. M. Eng, A. Bauer, A. Chacon, J. Kindervater, S. Mühlbauer, C. Pfleiderer, S. Buhrandt *et al.*, Unwinding of a skyrmion lattice by magnetic monopoles, Science **340**, 1076 (2013).

[13] K. Karube, J. S. White, N. Reynolds, J. L. Gavilano, H. Oike, A. Kikkawa, F. Kagawa, Y. Tokunaga, H. M. Rønnow, Y. Tokura *et al.*, Robust metastable skyrmions and their triangular–square lattice structural transition in a high-temperature chiral magnet, Nat. Mater. **15**, 1237 (2016).

[14] G. Berruto, I. Madan, Y. Murooka, G. M. Vanacore, E. Pomarico, J. Rajeswari, R. Lamb, P. Huang, A. J. Kruchkov, Y. Togawa *et al.*, Laser-induced skyrmion writing and erasing in an ultrafast cryo-Lorentz transmission electron microscope, Phys. Rev. Lett. **120**, 117201 (2018).

[15] B. Truc, A. A. Sapozhnik, P. Tengdin, E. Viñas Boström, T. Schönenberger, S. Gargiulo, I. Madan, T. LaGrange, A. Magrez, C. Verdozzi *et al.*, Light-induced metastable hidden skyrmion phase in the Mott insulator Cu_2OSeO_3, Adv. Mater. **35**, 2304197 (2023).

[16] M. Finazzi, M. Savoini, A. R. Khorsand, A. Tsukamoto, A. Itoh, L. Duo, A. Kirilyuk, T. H. Rasing, and M. Ezawa, Laser-induced magnetic nanostructures with tunable topological properties, Phys. Rev. Lett. **110**, 177205 (2013).

[17] K. Gerlinger, B. Pfau, F. Büttner, M. Schneider, L.-M. Kern, J. Fuchs, D. Engel, C. M. Günther, M. Huang, I. Lemesh *et al.*, Application concepts for ultrafast laser-induced skyrmion creation and annihilation, Appl. Phys. Lett. **118**, 192403 (2021).

[18] S.-G. Je, P. Vallobra, T. Srivastava, J.-C. Rojas-Sánchez, T. H. Pham, M. Hehn, G. Malinowski, C. Baraduc, S. Auffret, G. Gaudin *et al.*, Creation of magnetic skyrmion bubble lattices by ultrafast laser in ultrathin films, Nano Lett. **18**, 7362 (2018).

[19] L.-M. Kern, B. Pfau, M. Schneider, K. Gerlinger, V. Deinhart, S. Wittrock, T. Sidiropoulos, D. Engel, I. Will, C. M. Günther *et al.*, Tailoring optical excitation to control magnetic skyrmion nucleation, Phys. Rev. B **106**, 054435 (2022).

[20] L.-M. Kern, B. Pfau, V. Deinhart, M. Schneider, C. Klose, K. Gerlinger, S. Wittrock, D. Engel, I. Will, C. M. Günther *et al.*, Deterministic generation and guided motion of magnetic skyrmions by focused He^+-ion irradiation, Nano Lett. **22**, 4028 (2022).

[21] F. Büttner, B. Pfau, M. Böttcher, M. Schneider, G. Mercurio, C. M. Günther, P. Hessing, C. Klose, A. Wittmann, K. Gerlinger *et al.*, Observation of fluctuation-mediated picosecond nucleation of a topological phase, Nat. Mater. **20**, 30 (2021).

[22] C. Wang and Y. Liu, Ultrafast optical manipulation of magnetic order in ferromagnetic materials, Nano Convergence **7**, 1 (2020).

[23] R. Tomasello, E. Martinez, R. Zivieri, L. Torres, M. Carpentieri, and G. Finocchio, A strategy for the design of skyrmion racetrack memories, Sci. Rep. **4**, 1 (2014).

[24] B. Göbel and I. Mertig, Skyrmion ratchet propagation: Utilizing the skyrmion Hall effect in AC racetrack storage devices, Sci. Rep. **11**, 3020 (2021).

[25] P. Lai, G. Zhao, H. Tang, N. Ran, S. Wu, J. Xia, X. Zhang, and Y. Zhou, An improved racetrack structure for transporting a skyrmion, Sci. Rep. **7**, 1 (2017).

[26] G. Finocchio, M. Ricci, R. Tomasello, A. Giordano, M. Lanuzza, V. Puliafito, P. Burrascano, B. Azzerboni, and M. Carpentieri, Skyrmion based microwave detectors and harvesting, Appl. Phys. Lett. **107**, 262401-1 (2015).

[27] M. Mochizuki and S. Seki, Magnetoelectric resonances and predicted microwave diode effect of the skyrmion crystal in a multiferroic chiral-lattice magnet, Phys. Rev. B **87**, 134403 (2013).

[28] D. Prychynenko, M. Sitte, K. Litzius, B. Krüger, G. Bourianoff, M. Kläui, J. Sinova, and K. Everschor-Sitte, Magnetic skyrmion as a nonlinear resistive element: A potential building block for reservoir computing, Phys. Rev. Appl. **9**, 014034 (2018).

[29] D. Pinna, G. Bourianoff, and K. Everschor-Sitte, Reservoir computing with random skyrmion textures, Phys. Rev. Appl. **14**, 054020 (2020).

[30] K. M. Song, J.-S. Jeong, B. Pan, X. Zhang, J. Xia, S. Cha, T.-E. Park, K. Kim, S. Finizio, J. Raabe *et al.*, Skyrmion-based artificial synapses for neuromorphic computing, Nat. Electron. **3**, 148 (2020).

[31] J. Zázvorka, F. Jakobs, D. Heinze, N. Keil, S. Kromin, S. Jaiswal, K. Litzius, G. Jakob, P. Virnau, D. Pinna *et al.*, Thermal skyrmion diffusion used in a reshuffler device, Nat. Nanotechnol. **14**, 658 (2019).

[32] A. Bauer, M. Garst, and C. Pfleiderer, History dependence of the magnetic properties of single-crystal $Fe_{1-x}Co_xSi$, Phys. Rev. B **93**, 235144 (2016).

[33] M. Mochizuki, Spin-wave modes and their intense excitation effects in skyrmion crystals, Phys. Rev. Lett. **108**, 017601 (2012).

[34] Y. Onose, Y. Okamura, S. Seki, S. Ishiwata, and Y. Tokura, Observation of magnetic excitations of skyrmion crystal in a helimagnetic insulator Cu_2OSeO_3, Phys. Rev. Lett. **109**, 037603 (2012).

[35] T. Schwarze, J. Waizner, M. Garst, A. Bauer, I. Stasinopoulos, H. Berger, C. Pfleiderer, and D. Grundler, Universal helimagnon and skyrmion excitations in metallic, semiconducting and insulating chiral magnets, Nat. Mater. **14**, 478 (2015).

[36] J. D. Koralek, D. Meier, J. P. Hinton, A. Bauer, S. A. Parameswaran, A. Vishwanath, R. Ramesh, R. W. Schoenlein, C. Pfleiderer, and J. Orenstein, Observation of coherent helimagnons and Gilbert damping in an itinerant magnet, Phys. Rev. Lett. **109**, 247204 (2012).

[37] See Supplemental Material at http://link.aps.org/supplemental/10.1103/PhysRevApplied.21.034065 for more information on the temperature, magnetic field, and fluence dependence of the laser-written MSkL state, discussion of laser-heating effects, thermal modeling, and details of the spatially resolved measurements and modeling procedure.

[38] COMSOL Multiphysics ® v. 5.0. www.comsol.com. COMSOL AB, Stockholm, Sweden.